Resonances of a submerged fluid-filled spherically isotropic microsphere with partial-slip interface condition

Ganesh Tamadapu, Arne Nordmark, and Anders Eriksson

Resonances of a submerged fluid-filled spherically isotropic microsphere with partial-slip interface condition

Ganesh Tamadapu,[a)] Arne Nordmark,[b)] and Anders Eriksson[c)]
KTH Mechanics, Royal Institute of Technology, Osquars Backe 18, SE-100 44 Stockholm, Sweden

Motivated by the numerous applications of spherical shell models in micro and nano scales (such as microbubbles, bacterial cells, and viral capsids), we have considered the axisymmetric free vibrations of a spherically isotropic fluid-filled thick microspherical shell suspended in another unbounded fluid. A partial-slip condition is considered at the solid-fluid interface(s). Three-dimensional linear elasticity equations for the spherically isotropic shell dynamics and linearized Navier-Stokes equations for the two compressible viscous fluids are used in the analysis. The eigenvalue problem is discretized and solved to find the resonances and quality factors. A perfectly matched layer technique is used to separate the solid driven spectrum from the boundary reflecting spectrum. An example of air filled polymer shell suspended in water is presented. The added mass effect and partial-slip condition from water (air) on the frequencies and quality factors are found to be significant (negligible). Spherical isotropy is found to have major influence on the low frequency and large meridional wave number region of the resonance spectrum. High quality eigenmodes are observed due to very small viscous penetration depth compared to the shell size. In the thin-shell limit, the eigenvalue problem can have only two modes of vibration for any meridional wave number greater than or equal to two. This explains the reason for the second resonance frequency found for the quadrupole shape oscillations of various bacterium cells in the earlier work. The partial-slip condition is found to have very small influence on the first few modes of vibration. Surface tension is found to have significant influence only on the lowest frequency trend of the eigenspectrum. Perfectly matched layer technique used in the present analysis is found to be very effective in handling the boundary truncated problems. © *2015 AIP Publishing LLC.*
[http://dx.doi.org/10.1063/1.4926783]

I. INTRODUCTION

Submerged fluid-filled spherical shells can be found at different length scales in many modern engineering, biomedical, biological, and geophysical applications. In most of these applications, the dynamic behavior of the spherical shell with fluid coupling is of primary importance. Many researchers have studied the free vibrations of spherically isotropic (SI) macroscopic spherical shells with inviscid fluid coupling in various contexts.[1–3] It has been found that a spherical shell with few micrometers in outer diameter has fundamental frequencies in the ultrasound range. At micro scales, ultrasound has been shown to be an effective means for diagnostic ultrasound imaging,[4–7] killing bacteria,[8–12] deformation of cells,[13,14] and targeted drug delivery.[15–18] Many of the cells, microbubbles, and other microorganisms can also be modeled as fluid-filled submerged spherical shells. In a recent study, axisymmetric free vibrations of a viscous-fluid-filled piezoelectric thin spherical shell have been reported.[19] The effects from fluid interaction with the shell on the natural frequencies and damping components have been reported. It has been shown that the piezoelectric parameters have very little influence on the resonances of the shell. The quality of the natural vibrations of specified

bacteria cells has been investigated using a thin-shell model[12] by taking into account the elasticity of the shell (neglecting the inertia of shell) and inertial effects from the cytoplasm modeled as a fluid. The interaction of microbubbles with bacteria has been studied[20] using this thin-shell model.

In the past few decades, microbubbles have gained much attention due to their applications in the biomedical and biological fields as contrast agents for diagnostic ultrasound imaging.[4,21] More recently, contrast agents driven by ultrasound have been introduced for targeted drug delivery.[15] The strength of the driving pressure field and the frequency has critical influence on the behavior of the microbubble and its surroundings. These bubbles are coated with a stabilizing layer to avoid coalescence or dissolution during circulation. Typically, there are two types of coatings: flexible phospholipid coating or solid encapsulation (rigid coating), e.g., polymers. The coating thickness varies from application to application and depends on the coating material used. Flexibly coated microbubbles are a few nanometers in thickness. On the other hand, encapsulated microbubbles are hundreds of nanometers thick and their behavior observed in experiments is different from that of the bubbles with flexible coating.[15] Many models have been presented as an extension to Rayleigh-Plesset based equation to account for the shell rheology from these coatings.[22–27] However, no consensus exists on the best model to describe the observed

a)E-mail: tamadapu@kth.se
b)E-mail: nordmark@mech.kth.se
c)E-mail: anderi@kth.se

microbubble phenomena.[28] All the extended Rayleigh-Plesset models are useful in understanding the spherical oscillations of the microbubbles with various parameters. On the other hand, drug-delivery and other applications require good knowledge of phenomena like non-spherical oscillations, microstreaming, shear stress, and jetting. For the driving and excitation of these bubbles, good estimates for the mode shapes, resonances, and the quality factors associated with these modes are required.[29] These various applications of submerged fluid-filled spherical shell have motivated us to study the general free vibration analysis of a thick microspherical shell with viscous fluid interaction.

In this work, we have considered a fluid-filled thick spherical shell suspended in an unbounded fluid. We have primarily aimed at spheres of few micrometers in outer diameter. In many applications, proper estimation of shell linear resonances suffices to understand the experimentally observed behavior. In the present analysis, we have considered axisymmetric linear free vibrations of the shell. The two fluids inside and outside the shell are considered to be compressible and viscous, and can be of different properties. In reality, the shell is not isotropic and homogeneous. Hence, in the present analysis, the shell material is considered to be SI, which is transversely isotropic with a principal axis in the radial direction. The density of the shell is considered to be varying as a function of the radial coordinate, for instance, reflecting a variable porosity in the shell material. From the recent experimental, numerical, and theoretical investigations,[30] it has become apparent that the no-slip boundary condition at the solid-fluid interface is unphysical, especially, when considering micro and nano scales. Therefore, understanding of the solid-fluid interface boundary condition is becoming increasingly important.[31] For the present analysis, we have considered a partial-slip boundary condition at the solid-fluid interface which also reflects the porous flow of the inner and outer medium. The displacement vector field of the solid is expanded in terms of spherical harmonics with radial coordinate dependent amplitudes. Using these displacement fields in the three-dimensional elasticity equations for the linear shell dynamics, second order ordinary differential equations are obtained in the radial coordinate. Linearized Navier-Stokes equations are considered for the fluids inside and outside the shell. Using a Helmholtz decomposition, the axisymmetric first order velocity field of the fluid is decomposed using a scalar potential and a vector potential satisfying the solenoidal condition. The governing equations for the fluid potentials are obtained by expanding the potential fields in terms of spherical harmonics. The outer fluid boundary has been truncated for the purpose of numerical computation. To avoid reflections from the truncated boundary, we have introduced a perfectly matched layer ("PML")[32] at the truncated boundary. The six second order ordinary differential equations and twelve boundary conditions for the axisymmetric free vibration of the microsphere shell filled with a fluid and suspended in an unbounded fluid are discretized using a finite difference technique. The quadratic eigenvalue problem obtained after the discretization is solved to find the modes of vibration. The modes are characterized by the eigenfrequencies and quality factors. The PML method used here has been considered as very efficient in separating the actual eigenspectrum containing the solid driven modes from the spurious eigenspectrum containing the reflecting fluid modes. The present model is used to estimate the resonances of various bacterium cells, which is compared with the earlier results. The effect of spherical isotropy, partial-slip, surface tension, and density variation along the thickness on the resonances and qualities of microsphere modes is discussed.

The paper is organized as follows. In Section II, the mathematical formulation of the problem is presented. The solution method and quantitative analysis of mode shapes are presented in Section III. The numerical results and comparisons are presented and discussed in Section IV. The paper is concluded with Section V wherein some future directions are also indicated.

II. PROBLEM FORMULATION

Let $r, \theta,$ and φ be the radial, meridional, and azimuthal coordinates of the spherical coordinate system with orthonormal basis $(\boldsymbol{e}_r, \boldsymbol{e}_\theta, \boldsymbol{e}_\varphi)$, as shown in Fig. 1. Consider a thick microspherical shell of inner radius r_i and outer radius r_o. In most applications, the shell material is not isotropic and its properties change along the spherical layers. Therefore, we have considered a spherical shell with radially stratified isotropic material, also known as a SI material, with density varying as a function of the shell radial coordinate r. In other words, spherical isotropy implies that the elasticity of the shell is identical in all directions tangent to the spherical surface $r = $ constant. However, the formulation presented here can be extended to a shell with material properties varying radially.[33] The microsphere is filled with a fluid and is suspended in an other unbounded steady fluid. Both fluids, inside and outside the microsphere, are assumed to be compressible and viscous.

A. Solid governing equation

In most of the macro and micro applications, the density of the spherical shell is not uniform, but varies radially. In
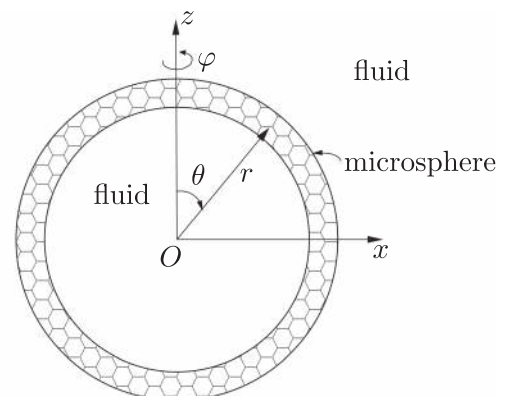

FIG. 1. A thick microspherical shell filled with a fluid and suspended in an other unbounded fluid.

the present analysis, the radial variation of shell density $\rho(r)$ is considered as

$$\rho(r) = \rho_s\left(1 + \frac{a(r - r_i)}{\rho_s(r - r_o + r_o b)}\right),$$

where a and b are two real constants and ρ_s is the shell density at the inner surface.

Let $\boldsymbol{u} = (u_r, u_\theta, u_\varphi)$ be the displacement vector field of the solid. The governing equation for a linear elastic spherical shell can be written as

$$\rho(r)\partial_t^2 \boldsymbol{u} = \nabla \cdot \boldsymbol{\sigma}_s, \tag{1}$$

where $\partial_t(\cdot) = \partial(\cdot)/\partial t$, ∇ is the gradient operator and $\boldsymbol{\sigma}_s$ is the linear stress tensor of the spherical shell. For a SI spherical shell, the components of the stress tensor can be expressed in terms of strain tensor ($\boldsymbol{\epsilon}$) components as

$$
\begin{aligned}
\sigma_{\theta\theta} &= c_{11}\epsilon_{\theta\theta} + c_{12}\epsilon_{\varphi\varphi} + c_{13}\epsilon_{rr}, \quad \sigma_{r\theta} = 2c_{44}\epsilon_{r\theta}, \\
\sigma_{\varphi\varphi} &= c_{12}\epsilon_{\theta\theta} + c_{11}\epsilon_{\varphi\varphi} + c_{13}\epsilon_{rr}, \quad \sigma_{r\varphi} = 2c_{44}\epsilon_{r\varphi}, \\
\sigma_{rr} &= c_{13}\epsilon_{\theta\theta} + c_{13}\epsilon_{\varphi\varphi} + c_{33}\epsilon_{rr}, \quad \sigma_{\theta\varphi} = 2c_{66}\epsilon_{\theta\varphi},
\end{aligned}
\tag{2}
$$

where, $c_{11}, c_{12}, c_{13}, c_{33}$, and c_{44} are the five elastic constants and $c_{66} = (c_{11} - c_{12})/2$. The necessary and sufficient conditions for positive definiteness of the fourth-order elasticity tensor relating the stress and strain are

$$
\begin{aligned}
c_{11} &> 0, \quad c_{11} > c_{12}, \quad c_{11}^2 > c_{12}^2, \\
c_{44} &> 0, \quad c_{33}(c_{11} + c_{12}) > 2c_{13}^2.
\end{aligned}
$$

We consider a radially inhomogeneous elastic material with spherical anisotropy restricted to SI, which is transverse isotropy with the principal axis as $\boldsymbol{e}_r$. Then, the time-harmonic displacement field $\boldsymbol{u}(r, \theta, \varphi, t)$ can be expanded in a separation of variables form with the dependence on θ and φ described by the spherical harmonics, with r-dependent amplitude.[33] Introducing the potentials[1,34] for the displacement field $\boldsymbol{u}(r, \theta, \varphi, t)$, we have

$$u_r = \chi, \quad u_\theta = -\frac{1}{\sin\theta}\partial_\varphi\Psi - \partial_\theta\Phi, \quad u_\varphi = \partial_\theta\Psi - \frac{1}{\sin\theta}\partial_\varphi\Phi. \tag{3}$$

For the axisymmetric vibration of the shell, the displacement field $\boldsymbol{u}$ is independent of the azimuthal coordinate φ. Therefore, the three field variables Ψ, Φ, and χ can be expressed as follows:[33]

$$
\begin{aligned}
\Psi(r, \theta, t) &= \sum_{n=1}^{\infty} \tilde{u}_n(r) P_n(\cos\theta) e^{st}, \\
\Phi(r, \theta, t) &= \sum_{n=1}^{\infty} \tilde{v}_n(r) P_n(\cos\theta) e^{st}, \\
\chi(r, \theta, t) &= \sum_{n=0}^{\infty} \tilde{w}_n(r) P_n(\cos\theta) e^{st},
\end{aligned}
\tag{4}
$$

where s is the eigenparameter and P_n is the Legendre polynomial of degree n. Substituting (2), (3), and (4) in (1), and using the orthogonality property of Legendre and associated

Legendre polynomials, gives the first order radial coordinate dependent equations

$$\left(\Delta_1 - \rho(\xi)s^2 - \frac{a_0^2}{\xi^2}\right)u_n = 0, \tag{5a}$$

$$\left(\Delta_1 - \rho(\xi)s^2 - \frac{a_1^2}{\xi^2}\right)v_n - \left((1 + c_3)\frac{1}{\xi}\frac{d}{d\xi} + \frac{a_2^2}{\xi^2}\right)w_n = 0, \tag{5b}$$

$$\left(c_4\Delta_1 - \rho(\xi)s^2 - \frac{a_3^2}{\xi^2}\right)w_n + n(n + 1)$$
$$\times \left((1 + c_3)\frac{1}{\xi}\frac{d}{d\xi} + \frac{a_4^2}{\xi^2}\right)v_n = 0, \tag{5c}$$

where $\Delta_1 = (1/\xi^2)(d/d\xi)(\xi^2(d/d\xi))$ and we have used the non-dimensional quantities

$$(u_n, v_n, w_n, \xi) = \frac{(\tilde{u}_n, \tilde{v}_n, \tilde{w}_n, r)}{r_o},$$

$$(c_1, c_2, c_3, c_4) = \frac{(c_{11}, c_{12}, c_{13}, c_{33})}{c_{44}},$$

$$\left(\lambda, \frac{1}{\tau}\right) = \left(s, \frac{1}{t}\right)\sqrt{\frac{r_o^2\rho_s}{c_{44}}}.$$

The constants, $a_0^2, a_1^2, a_2^2, a_3^2$, and a_4^2 are defined as

$$
\begin{aligned}
a_0^2 &= \frac{(c_1 - c_2)(n(n + 1) - 2) + 4}{2}, \\
a_1^2 &= (n(n + 1) - 1)c_1 + c_2 + 2, \quad a_2^2 = (2 + c_1 + c_2), \\
a_3^2 &= n(n + 1) + 2(c_1 - c_3 + c_2), \quad a_4^2 = c_3 - c_1 - c_2 - 1.
\end{aligned}
\tag{6}
$$

In general, Eqs. (5b) and (5c) are coupled except when $n = 0$, for which the equation is given by

$$\left(c_4\Delta_1 - \rho(\xi)s^2 - \frac{a_3^2}{\xi^2}\right)w_n = 0. \tag{7}$$

The non-dimensional radial and tangential components of the stress in the solid are given by

$$\sigma_{rr}^s = \left(2c_3w_0 + \xi c_4 w_0' + \sum_{n=1}^{\infty}(n(n + 1)c_3 v_n \right.$$
$$\left. + 2c_3w_n + \xi c_4 w_n')P_n(\cos\theta)\right)\frac{e^{\lambda\tau}}{\xi}, \tag{8}$$

$$\sigma_{r\theta}^s = \frac{1}{\xi}\sum_{n=1}^{\infty}(v_n + w_n - \xi v_n')P_n^1(\cos\theta)e^{\lambda\tau}, \tag{9}$$

where $(\cdot)' = d(\cdot)/d\xi$ and P_n^1 is the associated Legendre polynomial of first order and degree n.

B. Fluid governing equation

For the fluid motion set by the small amplitude vibrations of the shell, we have considered linearized Navier-Stokes equation along with equation of continuity and linearized state equation. As the size of the microsphere is much smaller than the sound wavelength, but much greater than

the viscous penetration depth, acoustic microstreaming phenomena can be observed away from the boundary layer, set by the attenuated acoustic energy in the boundary layer.[35,36] Therefore, the Reynolds number of the flow set by the solid away from the interface is not small for micro-scale objects, and to understand the fluid flow completely, one has to solve the Navier-Stokes equation for second order effects.[36] However, in the current analysis, for the linear free vibration of a shell, we restrict the study to first order effects in the fluid, to understand the resonances and quality factors of the mode shapes of vibration of the solid.

For small amplitude perturbations of the fluid, caused by the vibration of the shell, the equation of continuity can be written as follows:

$$\partial_t \rho_f + \rho_f (\mathbf{\nabla} \cdot \mathbf{v}) = 0, \tag{10}$$

and the linearized Navier-Stokes equation as

$$\rho_f \, \partial_t \mathbf{v} = \mathbf{\nabla} \cdot \boldsymbol{\sigma}_f. \tag{11}$$

Here, ρ_f is the perturbed fluid density, $\mathbf{v}$ is the first-order velocity field of the fluid, and $\boldsymbol{\sigma}_f$ is the fluid stress tensor given by

$$\boldsymbol{\sigma}_f = -p\,\mathbf{I} + \eta \left(\mathbf{\nabla} \mathbf{v} + \mathbf{\nabla} \mathbf{v}^T - \frac{2}{3}(\mathbf{\nabla} \cdot \mathbf{v})\mathbf{I} \right) + \eta^b (\mathbf{\nabla} \cdot \mathbf{v})\mathbf{I}, \tag{12}$$

where p is the perturbed fluid pressure, η and η^b are the shear and bulk viscosities of the fluid, and the linear equation of state is $p - p_0 = c_f^2 (\rho_f - \rho_{f_0})$, c_f is the speed of sound in the fluid, and p_0 and ρ_{f_0} are the equilibrium pressure and density, respectively. Using the expression for the oscillating acoustic pressure field $p = \tilde{p}\, e^{st}$ in the equations of state, (10) and (11), to eliminate $\tilde{p}$, the simplified first-order equation of motion for the fluid can be written as follows:

$$\rho_f \, \partial_t \mathbf{v} = \mathbf{\nabla}\left[\left(\frac{\rho_f c_f^2}{s} + \left(\eta^b + \frac{4}{3}\eta \right) \right) \mathbf{\nabla} \cdot \mathbf{v} \right] - \eta\, \mathbf{\nabla} \times \mathbf{\nabla} \times \mathbf{v}. \tag{13}$$

The first-order velocity field in the fluid can be written as the superposition of a potential part and a vorticity part, given by[35]

$$\mathbf{v} = s(\mathbf{\nabla}\phi + \mathbf{\nabla} \times \boldsymbol{\psi}), \tag{14}$$

where ϕ is the fluid scalar displacement potential field and $\boldsymbol{\psi}$ is the vorticity displacement potential field.

For the axisymmetric velocity field of the fluid, we can express the potentials as

$$\phi(r,\theta,t) = \sum_{n=0}^{\infty} \tilde{\phi}_n(r) P_n(\cos\theta) e^{st},$$

$$\boldsymbol{\psi}(r,\theta,t) = \mathbf{e}_\varphi \sum_{n=1}^{\infty} \tilde{\psi}_n(r) P_n^1(\cos\theta) e^{st}, \tag{15}$$

where $\mathbf{e}_\varphi$ is the unit azimuth vector of the spherical coordinate system. Substituting (14) and (15) into (13) and simplifying (taking divergence and curl), using the orthogonality property of Legendre and associated Legendre polynomials, gives the following uncoupled radial dependent non-dimensional equations of the fluid

$$\left(c^2 + \left(\gamma + \frac{4}{3}\beta \right) \frac{\lambda}{\rho} \right) \Delta_r \phi_n - \lambda^2 \phi_n = 0, \quad n \geq 0$$

$$\lambda \frac{\beta}{\rho} \Delta_r \psi_n - \lambda^2 \psi_n = 0, \quad n \geq 1, \tag{16}$$

where $\Delta_r = (\mathrm{d}^2/\mathrm{d}\xi^2) + (2/\xi)(\mathrm{d}/\mathrm{d}\xi) - n(n+1)/\xi^2$ and the non-dimensional parameters used are

$$\rho = \frac{\rho_f}{\rho_s}, \quad c = c_f \sqrt{\frac{\rho_s}{c_{44}}}, \quad (\beta,\gamma) = \frac{(\eta,\eta^b)}{r_o \sqrt{c_{44}\rho_s}},$$

$$(\phi_n,\psi_n) = \frac{\left(\tilde{\phi}_n, \tilde{\psi}_n \right)}{r_o^2}.$$

The non-dimensional radial and tangential velocity components of the fluid are given by

$$v_r = \lambda \phi_0' e^{\lambda\tau} - \lambda \sum_{n=1}^{\infty} \left(\phi_n' - \frac{n(n+1)}{\xi} \psi_n' \right) P_n(\cos\theta) e^{\lambda\tau}, \tag{17}$$

$$v_\theta = \frac{\lambda}{\xi} \sum_{n=1}^{\infty} (\phi_n - \psi_n - \xi\psi_n') P_n^1(\cos\theta) e^{\lambda\tau}. \tag{18}$$

The non-dimensional radial and tangential components of the stress in the fluid are given by

$$\sigma_{rr}^f = 2\beta\, \partial_\xi v_r + \left(\rho c^2 + \left(\gamma - \frac{2}{3}\beta \right) \lambda \right) \Delta_r \phi, \tag{19}$$

$$\sigma_{r\theta}^f = \beta \left(\frac{1}{\xi} \partial_\theta v_r + \partial_\xi v_\theta - \frac{v_\theta}{\xi} \right). \tag{20}$$

The surface tension pressure $\tilde{p}_{st}$ on the surface can be written as[36,37]

$$\tilde{p}_{st} = \frac{T_f}{r_o^2} \sum_{n=0}^{\infty} (n-1)(n+2) w_n P_n(\cos\theta) e^{\lambda\tau},$$

where $T_f = T_0/r_o c_{44}$ is the non-dimensional surface tension coefficient at the fluid-solid interface, and defined from the dimensional surface tension coefficient T_0.

Although the fluid outside the microsphere is considered to be unbounded, the computation has to be limited by truncating the outer boundary (Fig. 2). Because of the boundary truncation, there will be reflecting fluid modes from the truncated boundary which are of no interest. The "PMLs"[32] approach provides a convenient way to deal with these reflecting modes. Here, we will use a spherical coordinate

FIG. 2. Non-dimensional radial coordinate variation in different mediums.

system PML. The PML approximation can be seen as a complex shift in the coordinate system normal to the boundary.

Let $\xi_1(>1)$ and $\xi_2(\gg \xi_1)$ be the inner and outer radii of the PML. The complex shifting of the non-dimensional radial coordinate is given by $\tilde{\xi} = \xi(1 + i\tilde{\sigma}(\xi))$, where $\tilde{\sigma} \in C^2(\mathbb{R}^+)$ is a function satisfying

$$\tilde{\sigma}(\xi) = \begin{cases} 0 & \text{for } 1 < \xi < \xi_1 \\ \text{increasing} & \text{for } \xi_1 \leq \xi < \xi_2 \\ \sigma_0 & \text{for } \xi_2 \leq \xi, \end{cases} \quad (21)$$

where σ_0 is a real positive constant, which quantifies the damping of a PML layer. A typical C^2 function in $[\xi_1, \xi_2]$ with this property is given by[32]

$$\tilde{\sigma}(\xi) = \sigma_0 \frac{\int_{\xi_1}^{\xi} (x - \xi_1)^2 (\xi_2 - x)^2 dx}{\int_{\xi_1}^{\xi_2} (x - \xi_1)^2 (\xi_2 - x)^2 dx}.$$

The modified governing equations with the complex coordinate stretching for the fluid outside the microsphere can be written as

$$\left(c^2 + \left(\gamma + \frac{4}{3}\beta \right) \frac{\lambda}{\rho} \right) \tilde{\Delta}_r \phi_n - \lambda^2 \phi_n = 0, \quad n \geq 0$$

$$\lambda \frac{\beta}{\rho} \tilde{\Delta}_r \psi_n - \lambda^2 \psi_n = 0, \quad n \geq 1. \quad (22)$$

Here, $\tilde{\Delta}_r = \Delta_r$ for $1 \leq \xi < \xi_1$, and it is given by

$$\tilde{\Delta}_r = \frac{1}{p\tilde{p}^2\xi^2} \frac{d}{d\xi} \left(\frac{\tilde{p}^2 \xi^2}{p} \frac{d}{d\xi} \right) - \frac{n(n+1)}{\tilde{p}^2 \xi^2},$$

where $\tilde{p} = 1 + i\tilde{\sigma}$ and $p = \tilde{r}' = 1 + i\sigma$ with $\sigma = \tilde{\sigma} + i\tilde{\sigma}'$.

C. Boundary conditions

The classical no-slip boundary condition at the solid-fluid interface has been found to be unphysical in recent experimental studies at micro and nano scales,[30] and no consensus exists for the origin of this partial-slip condition. However, it has been observed in many experiments[30,38,39] that the surface slip velocity is in proportion to the local shear rate of the fluid. Therefore, the surface slip velocity can be expressed as

$$v_{\text{slip}} = \frac{L}{\beta} \sigma_{r\theta}^f,$$

where v_{slip} is the non-dimensional slip velocity of the fluid and L is the non-dimensional slip-length defined as the ratio of dimensional slip-length and outer radius of the shell.

In the present analysis, we are interested in studying the effect of partial-slip interface condition on the resonances and quality factors of the microspherical shell. The boundary conditions for the fluid inside the solid at $\xi = 0$ are

$\phi_n' = 0, \psi_n' = 0$. The boundary conditions at the fluid-solid interface $\xi = \xi_i$ and $\xi = 1$ are

$$v_r = \lambda u_r, \quad v_\theta - \lambda u_\theta = v_{\text{slip}}, \quad \sigma_{rr}^s = \sigma_{rr}^f - \tilde{p}_{st}^f, \quad \sigma_{r\theta}^s = \sigma_{r\theta}^f.$$

At the end of the PML $\xi = \xi_2$, we have considered simple Dirichlet boundary condition for both the potentials, $\tilde{\phi}_n = 0$ and $\tilde{\psi}_n = 0$.

III. SOLUTION METHOD

A. Discretization

Using the orthogonality property of the Legendre and associated Legendre polynomials, the governing equations for the solid and the fluid with boundary conditions in the radial directions can be separated. The radial coordinate dependent equations (5), (16), and (22) together with the boundary conditions for the vibration of a thick microspherical shell with fluid interaction are solved using a finite difference method (FDM). The equations are discretized using the central difference technique by replacing the zeroth, first, and second order derivatives of a field variable, say, V at a grid point m, with

$$V = V_m, \quad V' = \frac{V_{m+1} - V_{m-1}}{2h}, \quad V'' = \frac{V_{m+1} - 2V_m + V_{m-1}}{h^2}, \quad (23)$$

where h is the grid size, $\xi_{m+1} = \xi_m + h$, $m = 1, 2, 3, \ldots$

The non-dimensional radial coordinate ξ for the inner fluid $(0 < \xi \leq \xi_i)$, shell $(\xi_i \leq \xi \leq 1)$, and the outer fluid with PML $(1 \leq \xi \leq \xi_2)$ is divided into n_1, n_2, and n_3 intervals, respectively. Then, X_1, X_2, and X_3 are the corresponding nodal point vectors given by

$$X_1 = \{\phi_2, \phi_3, \ldots, \phi_{n_1+1}, \psi_2, \psi_3 \ldots, \psi_{n_1+1}\}^T,$$
$$X_2 = \{v_1, v_2 \ldots, v_{n_2+1}, w_1, w_2 \ldots, w_{n_2+1}\}^T, \quad (24)$$
$$X_3 = \{\tilde{\phi}_1, \tilde{\phi}_2 \ldots, \tilde{\phi}_{n_3+1}, \tilde{\psi}_1, \tilde{\psi}_2 \ldots, \tilde{\psi}_{n_3+1}\}^T.$$

The complete nodal vector can be written as $X = \{X_1^T, X_2^T, X_3^T\}^T$. As each nodal point has two field parameters, after excluding the $\xi = 0$ node using the zero gradient boundary condition, we thereby obtain $2(n_1 + n_2 + n_3 + 2)$ linear algebraic nodal equations. Using the twelve discretized boundary conditions, the unknown nodal field parameters in the boundary nodal equations are eliminated to obtain a linear matrix equation

$$A(\lambda) X = 0, \quad (25)$$

where $A(\lambda) = A_0 + A_1\lambda + A_2\lambda^2$ is the matrix quadratic polynomial in λ with coefficient matrices A_0, A_1, and A_2.

The quadratic eigenvalue problem (25) is rewritten in one of the two possible general eigenvalue problem forms as

$$\left[\begin{pmatrix} 0 & I \\ -A_0 & -A_1 \end{pmatrix} - \lambda \begin{pmatrix} I & 0 \\ 0 & A_2 \end{pmatrix} \right] \begin{bmatrix} X \\ \lambda X \end{bmatrix} = 0. \quad (26)$$

Solving the transformed eigenvalue problem (26) gives the eigenparameter λ and the eigenvector X.

B. Deformation measures

The strain tensor can be decomposed into two irreducible parts, namely, the dilatoric (trace part) and the deviatoric (trace free part) strain tensors as

$$\epsilon = \frac{1}{3}\vartheta\, I + \gamma,$$

where the trace of the strain tensor is the dilatation scalar $\vartheta = \mathrm{tr}(\epsilon)$ and γ is the trace-free deviatoric strain tensor. These tensors allow us to define two invariant deformation measures over the shell as follows.[40,41] The dilatoric measure may be defined as

$$J_\vartheta = \int\limits_0^{2\pi}\int\limits_0^{\pi}\int\limits_{r_i}^{r_o} \vartheta^2 r^2 \sin\theta\, \mathrm{d}r\, \mathrm{d}\theta\, \mathrm{d}\varphi,$$

which reflects the stretching of the shell. The deviatoric measure may be defined as

$$J_\sigma = \int\limits_0^{2\pi}\int\limits_0^{\pi}\int\limits_{r_i}^{r_o} \mathrm{tr}(\gamma^{\mathrm{T}}\gamma) r^2 \sin\theta\, \mathrm{d}r\, \mathrm{d}\theta\, \mathrm{d}\varphi,$$

which quantifies the amount of shear suffered by the shell. After finding the eigenvectors using the solution method presented above, the deformation measures are calculated by numerical integration to quantify the mode shapes in terms of the dilatoric and deviatoric components.

IV. RESULTS AND DISCUSSION

In the present analysis, we have considered an air-filled thick polymer shell submerged in water. For the present computation, the dimensional properties of the shell considered are the following: $r_o = 1.9\,\mu m$, $r_i = 1.5\,\mu m$, $\rho_s = 1296\,\mathrm{kg\,m^{-3}}$, $c_{44} = 7\,\mathrm{MPa}$, $T_0 = 0.075\,\mathrm{N\,m^{-1}}$. The dimensional properties of air are the following: $\rho_{\mathrm{air}} = 1.23\,\mathrm{kg\,m^{-3}}$, $\eta_{\mathrm{air}} = 1.8 \times 10^{-5}\,\mathrm{Pa\,s}$, $\eta^b_{\mathrm{air}} = 1.6 \times 10^{-5}\,\mathrm{Pa\,s}$, $c_{\mathrm{air}} = 343\,\mathrm{m\,s^{-1}}$, $L_{\mathrm{air}} = 100\,\mathrm{nm}$. The dimensional properties of water are the following: ρ_{water} $= 1000\,\mathrm{kg\,m^{-3}}$, $\eta_{\mathrm{water}} = 10^{-3}\,\mathrm{Pa\,s}$, $\eta^b_{\mathrm{water}} = 0.0026\,\mathrm{Pa\,s}$, $c_{\mathrm{water}} = 1500\,\mathrm{m\,s^{-1}}$, $L_{\mathrm{water}} = 33.33\,\mathrm{nm}$.

The non-dimensional parameters used for the computation are $\xi_i = 0.7895$, $\xi_0 = 1$, $\xi_1 = 4$, $\xi_2 = 10$, $a = 140.6$, $b = -0.1$, $c_1 = 55$, $c_2 = 50$, $c_3 = 50$, $c_4 = 62$, $\sigma_0 = 2$. For the case of isotropic material, c_{44} is the shear modulus and $c_4 = c_1 = c_2 + 2 = c_3 + 2 = 62$ (Poisson's ratio $\nu = 30/61$) is used in the computation.

The non-dimensional eigenparameter is complex and can be expressed as

$$\lambda = -\alpha + i\,\omega,$$

where ω is the angular frequency of oscillation and α is the decay rate of these oscillations. The decaying oscillation may be characterized by a quality factor given by[42]

$$Q = \frac{\omega}{2\alpha},$$

and the eigenparameter can thereby be rewritten as

$$\lambda = \omega\left(\frac{-1}{2Q} + i\right). \qquad (27)$$

Here, we use the dimensional frequency as $\Omega = \frac{\omega}{r_o}\sqrt{\frac{c_{44}}{\rho_s}}$.

A. Eigenspectrum

The eigenfrequencies for the variation of meridional wave numbers from $n = 1$ to $n = 15$ are shown in Fig. 3, for both isotropic and SI materials, for an air filled polymer shell suspended in unbounded water. As expected, the coupling between air and shell has very little influence on the eigenspectrum. The added mass effect from water on the eigenspectrum is also observed to be significant (result are not shown here), because of the higher water density compared to air density. We have considered the properties of SI material slightly deviated from the isotropic case. It is interesting to note that the SI eigenspectrum shows significant differences from the isotropic eigenspectrum in the large wave number region, Fig. 3(a), and low frequency region, Fig. 3(b).
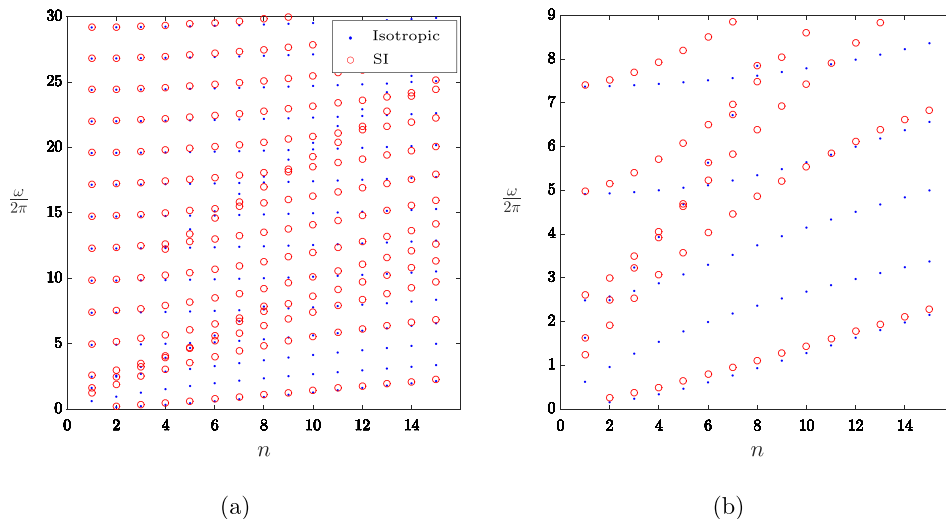

(a)

(b)

FIG. 3. (a) Variation of eigenfrequency $(\omega/2\pi)$ for the meridional wave number from $n = 1$ to $n = 15$, for isotropic and SI material cases. (b) Magnified view of the inset (a) in the low frequency range.
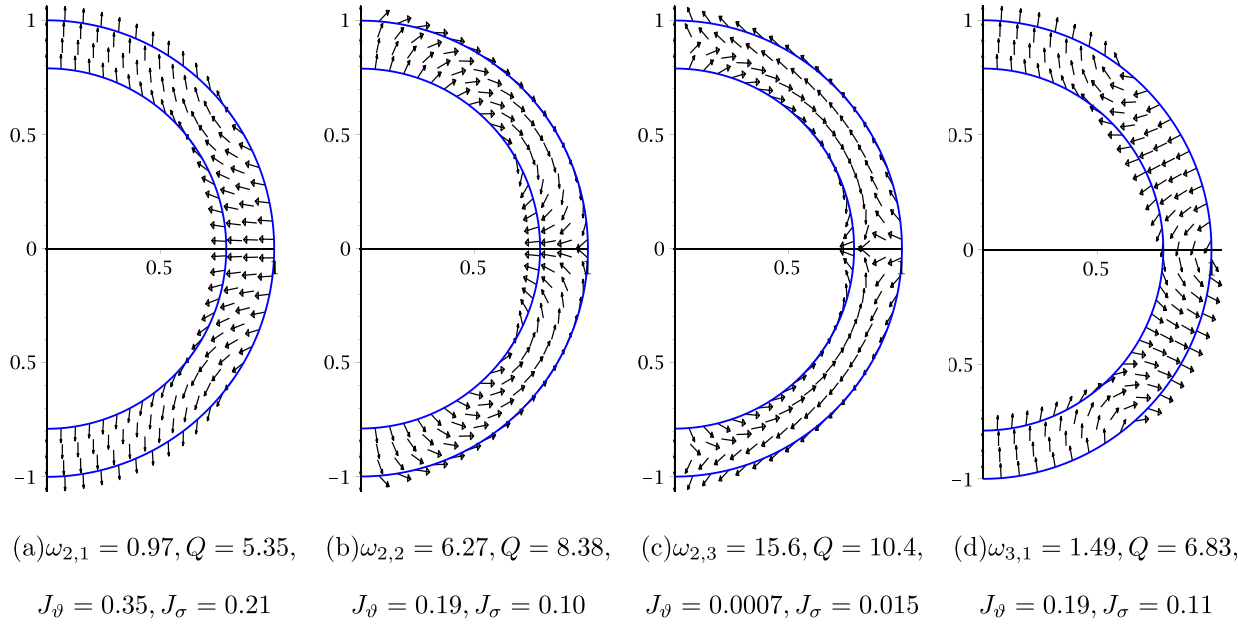
(a)$\omega_{2,1} = 0.97, Q = 5.35,$ (b)$\omega_{2,2} = 6.27, Q = 8.38,$ (c)$\omega_{2,3} = 15.6, Q = 10.4,$ (d)$\omega_{3,1} = 1.49, Q = 6.83,$

$J_\vartheta = 0.35, J_\sigma = 0.21$ $J_\vartheta = 0.19, J_\sigma = 0.10$ $J_\vartheta = 0.0007, J_\sigma = 0.015$ $J_\vartheta = 0.19, J_\sigma = 0.11$

FIG. 4. Vector field plots of different mode shapes for $n = 2$ and 3, and the corresponding eigenfrequencies and deformation measures.

The eigenspectrum has various non-crossing frequency trends along the meridional wave number (n), which are actually present in the shell eigenspectrum without fluid interaction. However, it is interesting to see two frequency trends which are crossing the non-crossing frequency trends. The first such crossing frequency trend (from $n = 1$ to $n = 8$) is almost unaffected by SI. The reason is that the mode shape corresponding to this frequency is a shear-dominated mode, similar to that shown in Fig. 4(c), with lower quality factor. On the other hand, the second crossing trend (starting at $n = 4$) is affected by SI.

All the frequencies shown are corresponding to solid modes with high quality factors. The first mode corresponding to meridional wave number $n = 0$ (purely radial

vibrations) with frequency $\Omega/2\pi = 12.42$ MHz has a very high quality factor $Q_0 = 89$. All the other eigenmodes for $n = 0$ are found to have quality factors less than five. However, the smallest eigenfrequency corresponds to $n = 2$. For $n = 2$, the first two modes do not have any spherical nodal surface/curve/point and they have quadrupole shape oscillations. The variations of the radial coordinate dependent normal and tangential displacements along the thickness of the shell and the fluid potentials are shown in Fig. 5, for the two quadrupole modes. For the first quadrupole mode in Fig. 4(a), the tip of the displacement vector at the top pole rotates through an angle of $-\pi/2$ when its tail moves from pole to equator. On the other hand, for the second quadrupole mode in Fig. 4(b), the tip of the displacement vector rotates

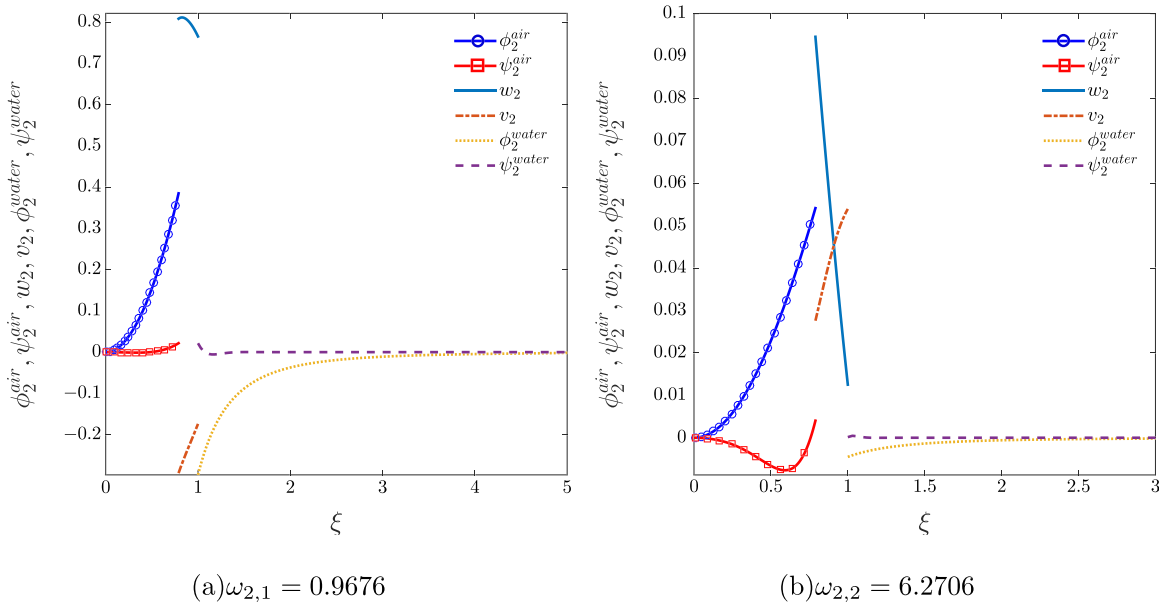(a)$\omega_{2,1} = 0.9676$ (b)$\omega_{2,2} = 6.2706$

FIG. 5. Variation of radial dependent amplitude functions for the two quadrupole mode shapes and the corresponding responses of air and water along the radial coordinate.

by an angle $3\pi/2$ when its tail moves from pole to the equator. The reason for this difference is that, for $n = 2$, the two radial coordinate dependent displacements v_2 and w_2 in Eq. (4), are in out-of-phase and in-phase for the first and second quadrupole modes, respectively, as shown in Fig. 5.

As the wavelength of sound waves is much longer than the size of the microsphere, purely radial modes can be excited very easily by a plane acoustic wave. On the other hand, for the excitation of non-spherical oscillations, breaking of spherical symmetry around the microsphere is required. However, in most of the applications, symmetry breaking is likely to occur due to the presence of microparticle cluster and wall effects.

With decrease in shell thickness, the variations along the thickness in Figs. 5(a) and 5(b) become almost independent of radial coordinate, but the phase difference still remains. This phase difference gives two eigenmodes in the thin-shell limit for $n > 1$. This explains why the two roots corresponding to a quadrupole mode shape observed[43,44] for the dispersion equation were presented to estimate the mechanical resonances of various cells using an isotropic thin-shell model.[12,45] Using the geometric and material properties of various bacteria cells,[12,44] the resonance calculations with the present model were performed, with some results. Properties of water are considered for fluids inside and outside the shell. For these calculations, the density of the shell is taken as $\rho_s = 10^{-9}$ kg m^{-3}. A non-dimensionalization used with the speed of sound in water to improve the condition of matrices $A_k, k = 0, 1, 2$ in Eq. (25). For the first quadrupole mode, the resonance calculations are in close match with Zinin et al.,[12] Choi et al.[44] and Zinin and Allen,[43] except for the E. coli and B. yeast cells due to inadequate surface tension data. For the second quadrupole mode, the resonances are in good match,[44] where the authors concluded that the quadrupole mode shape has more than one natural frequency, but with several quality factors. However, from our calculations, the cells can have only two quadrupole mode shapes with different resonances and quality factors. The minor discrepancies of the present calculations from the literature data are due to the numerical difficulties in applying this model to very thin shells with negligible inertia and truncated boundary conditions (Table I).

For the isotropic/SI material case, the first mode corresponding to $n = 3$ has octupole shape and its vector field plot for the isotropic case is shown in Fig. 4(d). For $n = 1$, the mode shape with displacement field along the thickness, similar to that shown in Fig. 5(a), cannot exist.[41] From the values of J_ϑ and J_σ, the mode shapes shown in Figs. 4(a), 4(b), and 4(d) are mixed modes. On the other hand, the mode shape in Fig. 4(c) is very close to a pure shear mode.

B. Quality factors

As reported in the previous studies, the viscous shear waves are the main source of dissipation of microsphere oscillations. The influence of viscosity on the shell vibration can be understood from the relation between the size of the microsphere and the viscous penetration depth $\delta = \sqrt{2\eta/\rho_f\Omega}$. For $\delta > r_o$, the viscous shear wave effect will be present for more volume around the shell, and the modes of vibration are damped effectively. For $\delta < r_o$, the damping effect is very small on the shell oscillations. The variation of non-dimensional eigenfrequency $\omega/2\pi$ and the corresponding quality factor Q for $n = 2$ is shown in Fig. 6(a) for a SI material. The magnified plot for the first few resonances is shown in Fig. 6(b). Considering base model as partial-slip interface condition, these are shown for calculation based on various conditions like no-slip of water, no-slip of air, no-slip, no surface tension, and average shell density (1183.6 kg m^{-3}). The horizontal dotted lines in Fig. 6 correspond to shell frequencies without these two fluids. The microsphere is found to have very high quality factors. This can be understood by finding the critical frequency ($\omega_c/2\pi$), for which the viscous penetration depth becomes equal to the outer radius of the shell. For the present study, the non-dimensional frequency $\omega_c/2\pi = 0.00226$, which is much lower than the fundamental non-dimensional frequency of the shell.

It is interesting to note that the relation between quality factor and eigenfrequency is almost linear or even proportional for the frequency range shown in Fig. 6(a), except for the few lowest frequency modes. However, the region for which this linear relationship holds is highly dependent on shear viscosity. The slope of the line for the partial-slip condition is lower than for the no-slip condition in Fig. 6(a).

TABLE I. Natural frequencies $\Omega_2/2\pi$ (MHz) and quality factors Q_2 for the quadrupole oscillations for different bacterial cells. Comparison of present model calculations with Zinin et al.,[12] Choi et al.,[44] and Zinin and Allen[43] are also given in this table. μ : cell's shell shear modulus, ν : Poisson's ratio, and h : cell's shell thickness.

Cell type[12]	r_o (μm)	h (nm)	μ (MPa)	ν	$\frac{\Omega_2}{2\pi}$	Q_2	$\frac{\Omega_2}{2\pi}$ (Refs. 12 and 43)	Q_2	$\frac{\Omega_2}{2\pi}$ (Ref. 44)	Q_2
E. coli	0.5	6	10.7	0.16	3.61	0.74	4.58	0.63	3.62	0.63
					14.4	0.49	…	…	14.4	0.49
C. eugametos	8	60	433.5	0.49	3.53	15.31	3.41	15.7	…	…
					28.92	0.37	…	…	…	…
B. emersonii	10	450	47.7	0.49	2.34	16.7	2.24	15.8	2.24	16.0
					23.81	0.48	…	…	24.2	0.9
D. carota	30	100	308	0.49	0.532	23.0	0.517	23.2	0.517	23.5
					7.7	0.5	…	…	7.0	0.9
B. yeast	4.5	100	0.2	0.5	0.247	3.23	0.16	1.2	0.16	1.6
					0.579	0.66	…	…	0.584	0.6

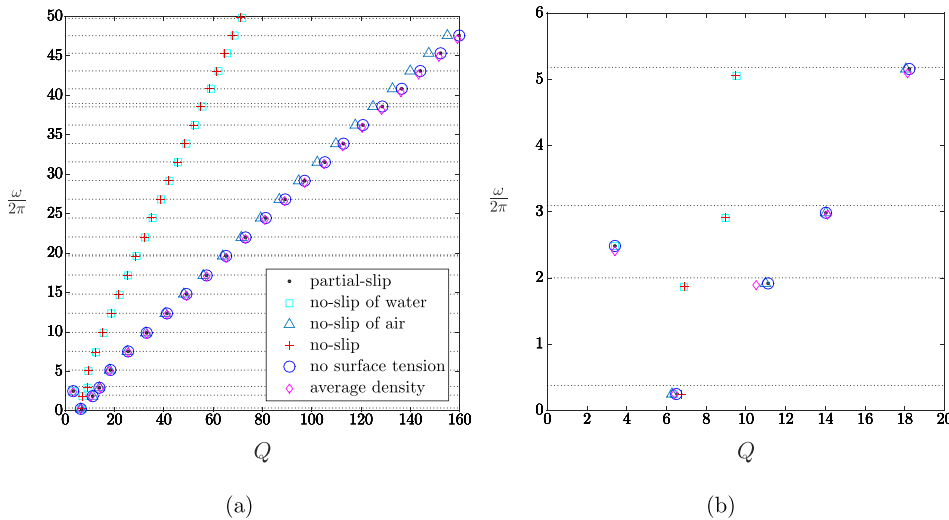(a)   (b)

FIG. 6. Eigenfrequency $\omega/2\pi$ and the corresponding quality factor Q of SI shell for $n=2$ (with base model as partial-slip interface condition) for various conditions like no-slip of water, no-slip of air, no-slip, no surface tension, and average density of the shell. The horizontal dotted lines correspond to eigenfrequencies of the SI shell without fluid interaction. In inset (a), the cluster of points falling approximately on the line with smaller slope has major influence from the partial-slip of water. The line with larger slope corresponds to no-slip interface condition.

This is due to the fact that the partial-slip condition helps in reducing the dissipation of energy. The partial-slip at the inner (outer) boundary from air (water) has minor (major) influence on the quality of the microsphere resonances. It is interesting to note that the first crossing frequency trend in Fig. 3 occurs only when there is a partial-slip condition from gas and is independent of the partial-slip from water. This trend disappears for the no-slip interface condition. As expected, the partial-slip condition also increases the frequency due to the reduced fluid inertial effects; this is, however, not significant (0.1 MHz and 1.1 MHz for the first and second quadrupole modes, respectively). We have also observed that the resonances of the system are not strongly affected by the surface tension,[12] except for the first quadrupole mode. For the first quadrupole mode shape of the isotropic shell, increasing the surface tension T_0 at the outer surface interface ($T_0 = 0$ at the inner surface interface) from 0.075 to 0.75 N m^{-1} increases the corresponding dimensional frequency (quality factor) from 6.13 MHz (5.35) to 7.17 MHz (5.8). On the other hand, further increase in the surface tension has negligible influence on the second quadrupole mode and other higher modes. This has been also observed[44] for the second quadrupole mode shape of an *E. coli* cell. This surface tension effect is observed for the lowest frequency trend in the eigenspectrum, starting with the first quadrupole mode. The density variation along the thickness has very small influence on the resonances, when compared with the average shell density calculations.

C. Effect of PML

The resonance spectrum for a meridional wave number $n=2$ is shown in Fig. 7 for two cases of computations, namely, without PML ($\sigma_0 = 0$) and with PML ($\sigma_0 = 2$), at the truncated boundary. As the PML introduces a complex coordinate system, the eigenspectrum is not symmetric about the horizontal axis. However, the solid driven frequencies shown in Fig. 3 correspond to a group of points close to the origin in Fig. 7, and are nordat all influenced by the PML. On the other hand, the points corresponding to the reflecting modes are breaking the symmetry. With the introduction of PML, these points in the upper (lower) left-half of the

complex plane start moving towards (away from) the real axis. In this way, the actual resonance spectrum is efficiently separated from the spurious/reflecting spectrum by the perfectly matched layer technique. The movement/separation of these points is highly dependent on the attenuation parameter σ_0 and also on the PML thickness. However, it is not possible to eliminate the complete spurious spectrum. The best value of σ_0 can be decided by few numerical experiments and it has an inverse relationship with the damping present in the system. As the attenuation of waves entering into the PML is frequency dependent, few low frequency (large wave length) reflecting modes are not separated from the actual spectrum, even with a large PML thickness. However, for $\alpha/2\pi < 4$, we have achieved very good separation of the solid driven spectrum from the boundary reflecting spectrum. Cases can be found, by changing the problem parameters, for which solid driven spectrum and reflecting spectrum overlap, and PML technique is very useful in the separation of such spectra. When solving the problem without PML, we have used the condition of no backward traveling longitudinal waves and zero shear stress at the truncated boundary.
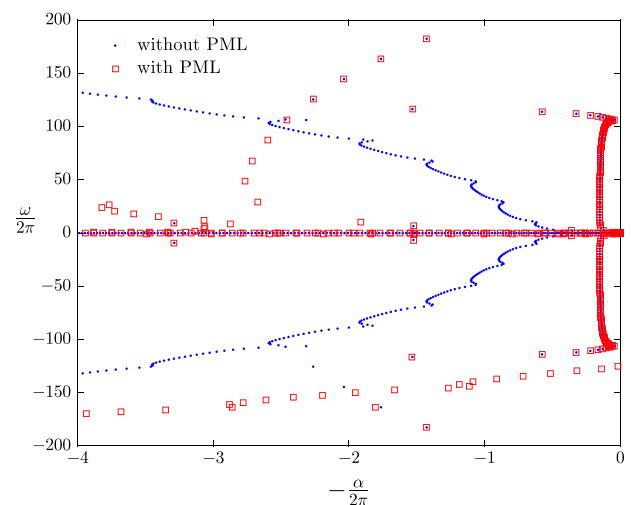

FIG. 7. Eigenspectrum for a meridional wave number $n=2$ without PML ($\sigma_0 = 0$) and with PML ($\sigma_0 = 2$).

V. CONCLUSIONS

Axisymmetric free vibrations of a fluid-filled thick microspherical shell suspended in another fluid is considered in the present analysis. A model for finding the eigenfrequencies and quality factors for the linear vibrations of a SI shell with partial-slip solid-fluid interface condition is presented for two compressible viscous fluids. The quality factors of the natural vibrations of the shell are found by solving the eigenvalue problem for an air-filled thick polymer microspherical shell suspended in water. High quality resonances are observed due to the very small viscous penetration depth compared to the shell radius. The added mass effect and partial-slip of water (air) have major (minor) influence on the resonance spectrum. The effect of partial-slip on the first few fundamental modes is found to be very low. The density variation along the thickness has very little influence on the resonances when compared with the average density calculations. The surface tension has very little influence on the eigenspectrum, except for the fundamental frequency trend starting with first quadrupole mode. The perfectly matched layer technique, used in the computation to handle the truncated boundary, is found to be very efficient in separating the solid driven resonance spectrum from the spurious/reflecting spectrum.

For the thin-shell limit, the problem reduces to an eigenvalue problem of dimension two for any meridional wave number $n \geq 2$. Using this model for the thin-shell limit, resonances and quality factors are calculated for the two quadrupole shapes for various bacteria and compared with previous studies. We have also explained the deformation pattern of these modes which were not clear in the earlier studies.[12,43,44] Certain invariant deformation measures are calculated to quantify the mode shapes in terms of the dilatoric and deviatoric components present.

The model presented can be extended to study the resonance and quality factors of a shell with elastic and viscous properties varying radially. Parametric analysis can be done with this model for various applications with different geometric and material properties of the shell and fluids. Further, nonlinear analysis of submerged fluid-filled microspherical shell with size dependent material properties is required for various applications.[15,21]

ACKNOWLEDGMENTS

[1]W. Q. Chen and H. J. Ding, J. Acoust. Soc. Am. **105**, 174 (1999).
[2]W. Q. Chen, X. Wang, and H. J. Ding, J. Acoust. Soc. Am. **106**, 2588 (1999).
[3]W. Q. Chen, J. B. Cai, G. R. Ye, and H. J. Ding, ASME J. Appl. Mech. **67**, 422 (2000).
[4]E. Stride and N. Saffari, Proc. Inst. Mech. Eng., Part H **217**, 429 (2003).
[5]S. Zhao, K. W. Ferrara, and P. A. Dayton, Appl. Phys. Lett. **87**, 134103 (2005).
[6]L. Hoff, *Acoustic Characterization of Contrast Agents for Medical Ultrasound Imaging* (Kluwer, Dordrecht, 2001).
[7]T. Faez, M. Emmer, K. Kooiman, M. Versluis, A. Van Der Steen, and N. De Jong, IEEE Trans. Ultrason. Ferroelectr. Freq. Control **60**, 7 (2013).
[8]E. Joyce, S. S. Phull, J. P. Lorimer, and T. J. Mason, Ultrason. Sonochem. **10**, 315 (2003).
[9]T. Blume and U. Neis, Ultrason. Sonochem. **11**, 333 (2004).
[10]K. Hoover, M. Bhardwaj, N. Ostiguy, and O. Thompson, Mater. Res. Innov. **6**, 291 (2002).
[11]P. V. Zinin, Ultrasonics **30**, 26 (1992).
[12]P. V. Zinin, J. S. Allen, and V. M. Levin, Phys. Rev. E **72**, 061907 (2005).
[13]P. Marmottant and S. Hilgenfeldt, Nature **423**, 153 (2003).
[14]H. Chen, W. Kreider, A. A. Brayman, M. R. Bailey, and T. J. Matula, Phys. Rev. Lett. **106**, 034301 (2011).
[15]K. Kooiman, H. J. Vos, M. Versluis, and N. de Jong, Adv. Drug Delivery Rev. **72**, 28 (2014).
[16]S. Hernot and A. L. Klibanov, Adv. Drug Delivery Rev. **60**, 1153 (2008).
[17]K. Hynynen, Adv. Drug Delivery Rev. **60**, 1209 (2008).
[18]K. Tachibana and S. Tachibana, Jpn. J. Appl. Phys., Part 1 **38**, 3014 (1999).
[19]J. Hu, Z. Qiu, and T. C. Su, J. Sound Vib. **330**, 5982 (2011).
[20]P. V. Zinin and J. S. Allen, Phys. Rev. E **79**, 021910 (2009).
[21]A. A. Doinikov and A. Bouakaz, IEEE Trans. Ultrason. Ferroelectr. Freq. Control **58**, 981 (2011).
[22]C. C. Church, J. Acoust. Soc. Am. **97**, 1510 (1995).
[23]L. Hoff, P. C. Sontum, and J. M. Hovem, J. Acoust. Soc. Am. **107**, 2272 (2000).
[24]K. Sarkar, W. T. Shi, D. Chatterjee, and F. Forsberg, J. Acoust. Soc. Am. **118**, 539 (2005).
[25]S. M. van der Meer, B. Dollet, M. M. Voormolen, C. T. Chin, A. Bouakaz, N. de Jong, M. Versluis, and D. Lohse, J. Acoust. Soc. Am. **121**, 648 (2007).
[26]K. Tsiglifis and N. A. Pelekasis, J. Acoust. Soc. Am. **123**, 4059 (2008).
[27]A. A. Doinikov, J. F. Haac, and P. A. Dayton, Ultrasonics **49**, 269 (2009).
[28]T. Faez, M. Emmer, K. Kooiman, M. Versluis, A. van der Steen, and N. de Jong, IEEE Trans. Ultrason. Ferroelectr. Freq. Control **60**, 7 (2013).
[29]D. Grishenkov, C. Pecorari, T. B. Brismar, and G. Paradossi, Ultrasound Med. Bio. **35**, 1127 (2009).
[30]E. Lauga, M. Brenner, and H. A. Stone, in *Springer Handbook of Experimental Fluid Mechanics* (Springer Berlin Heidelberg, 2007), pp. 1219–1240.
[31]S. Hanot, M. Belushkin, and G. Foffi, Soft Matter **9**, 291 (2013).
[32]S. Kim and J. E. Pasciak, Math. Comput. **78**, 1375 (2009).
[33]A. N. Norris and A. L. Shuvalov, Proc. R. Soc. London, Ser. A **468**, 467 (2011).
[34]J. N. Sharma and N. Sharma, ASME J. Appl. Mech. **77**, 021004 (2010).
[35]L. D. Landau and E. M. Lifshitz, *Fluid Mechanics* (Pergamon Press, 1959), Vol. 6.
[36]A. A. Doinikov and A. Bouakaz, J. Acoust. Soc. Am. **127**, 1218 (2010).
[37]H. W. Jackson, M. Barmatz, and C. Shipley, J. Acoust. Soc. Am. **84**, 1845 (1988).
[38]P. A. Thompson and S. M. Troian, Nature **389**, 360 (1997).
[39]Y. Zhu and S. Granick, Phys. Rev. Lett. **87**, 096105 (2001).
[40]G. Tamadapu and A. DasGupta, Int. J. Eng. Sci. **60**, 25 (2012).
[41]A. DasGupta and G. Tamadapu, Eur. J. Mech. A: Solids **39**, 280 (2013).
[42]I. Main, *Vibrations and Waves in Physics* (Cambridge University Press, 1993).
[43]P. V. Zinin and J. S. Allen, Phys. Rev. E **82**, 033901 (2010).
[44]Y. Choi, W.-S. Ohm, and Y.-T. Kim, Phys. Rev. E **82**, 013901 (2010).
[45]P. V. Zinin, V. M. Levin, and R. G. Maev, Biophys. J. **32**, 202 (1987).